iScience

CellPress
OPEN ACCESS

Article

# High cardiomyocyte diversity in human early prenatal heart development

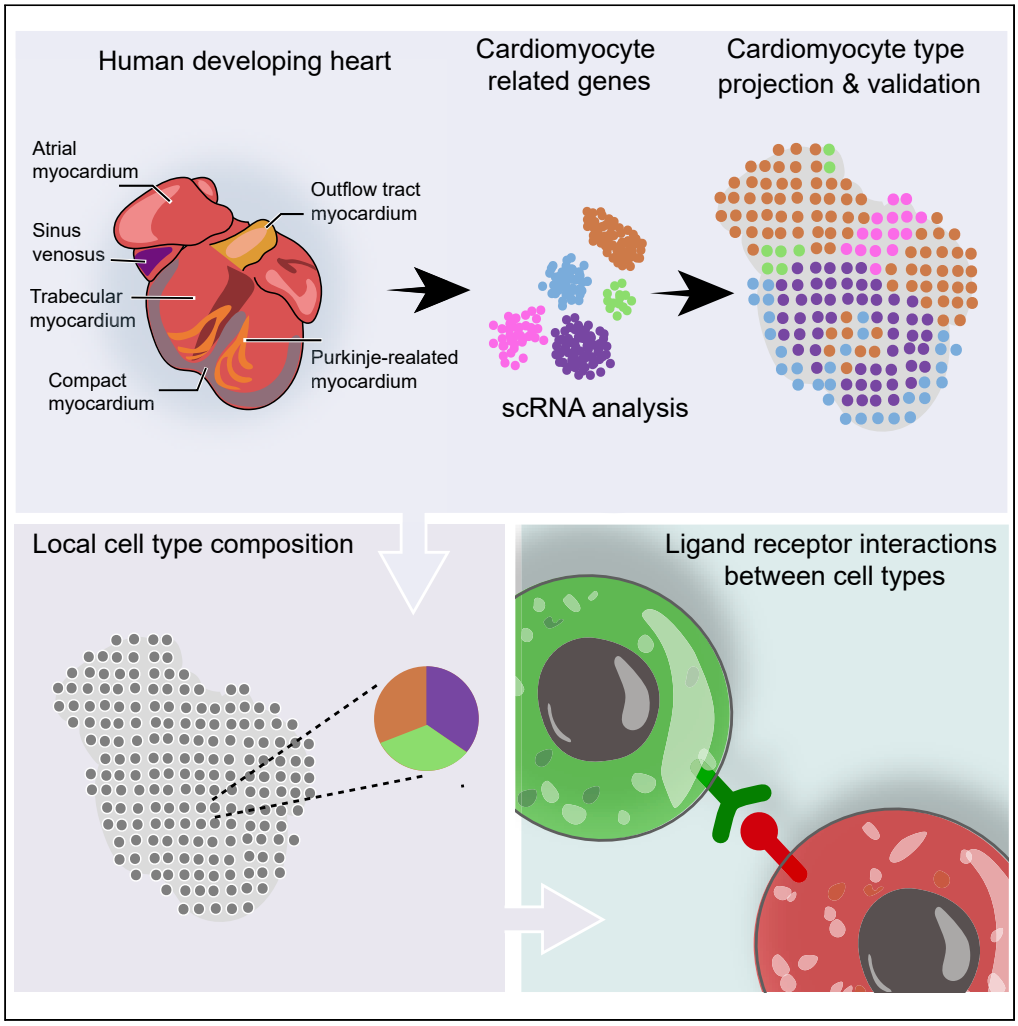


Christer Sylvén, Eva Wärdell, Agneta Månsson-Broberg, ..., Ludvig Larsson, Åsa Björklund, Stefania Giacomello

christer.sylven@ki.se (C.S.)
stefania.giacomello@scilifelab.se (S.G.)

## Highlights

Specific spatial locations for human prenatal cardiomyocyte (CMs) phenotypes

Heterogeneity in mitochondrial and connexin expression in human prenatal CMs

Less ligand-receptor interactions in human prenatal CMs than in non-CMs

Substantial integrin ligand-receptor interactions with human prenatal CMs

Sylvén et al., iScience *26*, 105857
January 20, 2023 
https://doi.org/10.1016/j.isci.2022.105857

iScience

CellPress
OPEN ACCESS

Article

# High cardiomyocyte diversity in human early prenatal heart development

Christer Sylvén,[1,*] Eva Wärdell,[1] Agneta Månsson-Broberg,[1] Eugenio Cingolani,[2] Konstantinos Ampatzis,[3] Ludvig Larsson,[4] Åsa Björklund,[5] and Stefania Giacomello[4,6,*]

## SUMMARY

**Cardiomyocytes play key roles during cardiogenesis, but have poorly understood features, especially in prenatal stages. Here, we characterized human prenatal cardiomyocytes, 6.5–7 weeks post-conception, by integrating single-cell RNA sequencing, spatial transcriptomics, and ligand-receptor interaction information. Using a computational workflow developed to dissect cell type heterogeneity, localize cell types, and explore their molecular interactions, we identified eight types of developing cardiomyocyte, more than double compared to the ones identified in the *Human Developmental Cell Atlas*. These have high variability in cell cycle activity, mitochondrial content, and connexin gene expression, and are differentially distributed in the ventricles, including outflow tract, and atria, including sinoatrial node. Moreover, cardiomyocyte ligand-receptor crosstalk is mainly with non-cardiomyocyte cell types, encompassing cardiogenesis-related pathways. Thus, early prenatal human cardiomyocytes are highly heterogeneous and develop unique location-dependent properties, with complex ligand-receptor crosstalk. Further elucidation of their developmental dynamics may give rise to new therapies.**

## INTRODUCTION

Cardiomyocytes (CMs) are the contracting units of the heart. Their growth and adaptation are seminal for cardiogenesis during early prenatal development, when the heart has transformed from a primitive heart tube to a growing four-chambered heart and outflow parts of the ventricles are developing.[1–3] Elements of the venous pole of the cardiac tube and cardiac mesenchyme related to the sinus venosus, great cardiac veins, and pulmonary veins develop into the trabeculated atrial appendages, atrial septum, central conduit part of the atria, and sinoatrial node (SAN), from which the normal heart beat originates.[1,4–7] The atrial structures originating from the great cardiac and pulmonary veins are myocardialized by CMs,[8,9] which form the smooth-walled conduit parts of the atria.

However, the mechanisms involved in cell division, differentiation with development of contractility, energy production, and electrical integrity of cardiomyocytes in these developmental compartments are still unknown. Thus, exploration of CMs' spectrum, specification, growth, and interactions with other cells during early prenatal life is needed to improve understanding of cardiac health, the development of CM populations, and thus potential avenues toward new regenerative therapies for heart failure.

Asp et al. (2019) have generated the most comprehensive spatial cell atlas, at the time of writing, of human prenatal heart development between 4.5 and 9 post-conceptional weeks (PCW) using spatial transcriptomics (ST),[10,11] single-cell RNA sequencing (scRNA-seq),[12] and *in situ* sequencing data.[13,14] This dataset forms part of the *Human Developmental Cell Atlas* (*HDCA*). At 6.5–7 PCW, Asp et al. (2019) identified three CM populations, corresponding to atrial CMs, ventricular CMs, and MYOZ2-enriched CMs. Here, we present a high-resolution characterization of the CM populations at 6.5–7 PCW, achieved by applying a computational workflow developed to dissect and characterize cell type heterogeneity, localize the cell types, and explore their ligand-receptor (L-R) interactions.

## RESULTS

We initially applied Uniform Manifold Approximation and Projection (UMAP)[15] for dimensionality reduction and clustering of the *HDCA* 6.5–7 PCW heart scRNA-seq dataset[16] (Figure S1A). To specifically investigate the CM

[1]Department of Medicine, Karolinska Institute, Huddinge, Sweden

[2]Cedars-Sinai, Smidt Heart Institute, Los Angeles, CA, USA

[3]Department of Neuroscience, Karolinska Institute, Stockholm, Sweden

[4]Science for Life Laboratory, Department of Gene Technology, KTH Royal Institute of Technology, Stockholm, Sweden

[5]Department of Cell and Molecular Biology, National Bioinformatics Infrastructure Sweden, Science for Life Laboratory, Uppsala University, Uppsala, Sweden

[6]Lead contact

*Correspondence: christer.sylven@ki.se (C.S.), stefania.giacomello@scilifelab.se (S.G.)

https://doi.org/10.1016/j.isci.2022.105857

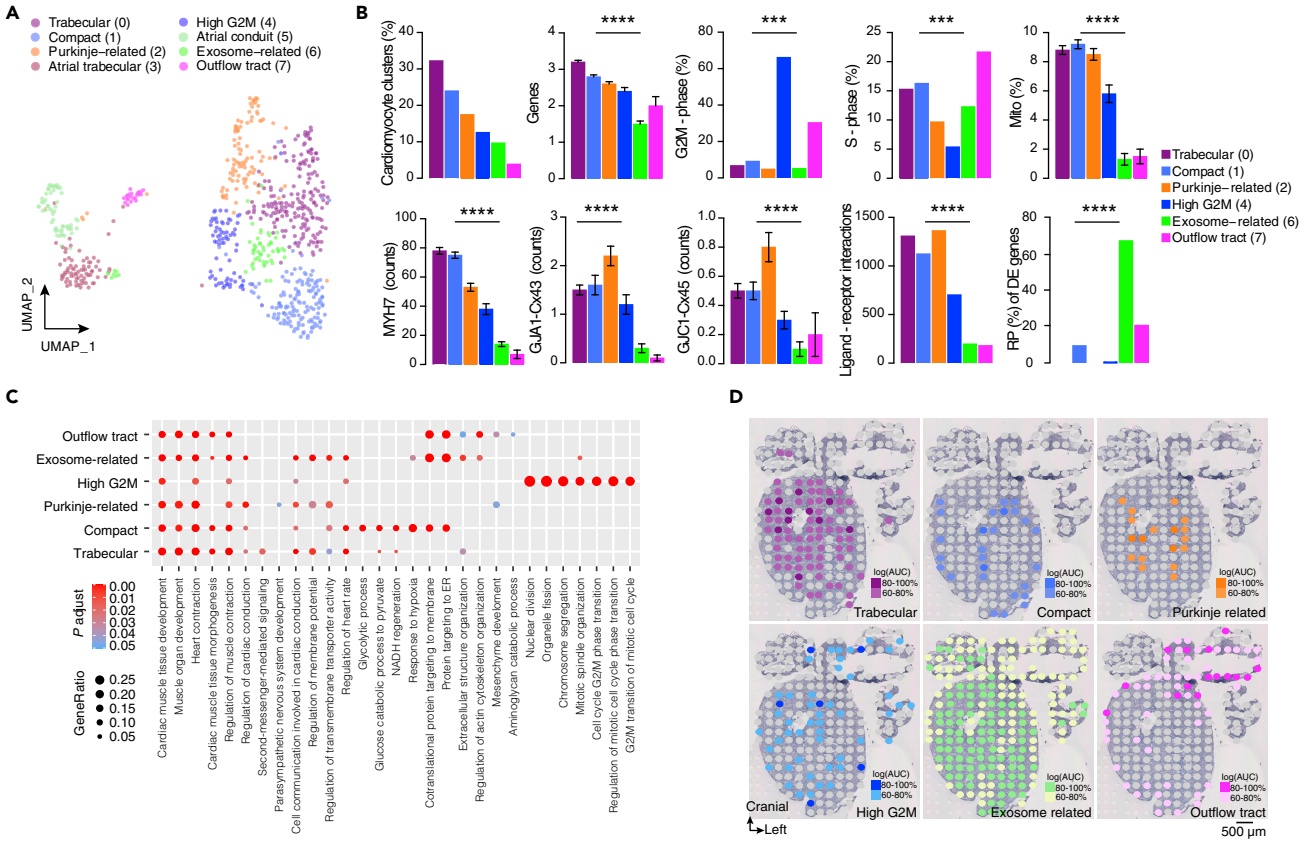


**Figure 1. Basic properties of ventricular cardiomyocyte types**

(A) Two-dimensional UMAP of scRNA-seq ventricular and atrial CM clusters.

(B) Summary of basic properties of ventricular CM types: percentage of total, number of genes ×1000, percentages of cells in G2M and S phases, percentage of mitochondrial RNA, counts of *MYH7*, connexins *GJA1* (Cx43) and *GJC1* (Cx45), number of L-R interactions, and percentage ribosomal proteins of DE genes. Asterisks indicate *p* values obtained from one-way ANOVA or chi-square tests on absolute numbers: ***p < 0.0005; ****p < 0.0001.

(C) GO: biological processes.

(D) Deconvolution of ventricular CM types and their locations on an ST map.

heterogeneity of the human prenatal heart, we subclustered 726 cells corresponding to the three CM clusters identified in the *HDCA* dataset, i.e., ventricular, atrial, and *MYOZ2*-enriched CMs. Through this process, eight CM clusters emerged (Figure 1A; Figure S1B). Of these, six (designated clusters 0–2, 4, 6, and 7) were ventricular CM clusters expressing *MYH7* and two (clusters 3 and 5) were atrial CM clusters expressing *MYH6*.

## Characteristics of ventricular cardiomyocyte populations

The three largest ventricular CM clusters (clusters 0, 1, and 2; Figures 1A and 1B) contained ≈75% of the cells, with higher mitochondrial content, connexin expression, and L-R interactions than cells in the other three ventricular CM clusters (4, 6, and 7). This suggests they were more mature and morphologically integrated with higher oxidative, contractile, and electrical conductivity capacities.[17,18]

The third largest cluster (cluster 2) was associated with strong differential expression (DE) of the gene *IRX3*, with an adjusted p value (p_val_adj) of $4.8 \times 10^{-17}$ (Figures S2A and S2B), which is characteristic of the distal part of the Purkinje fibers.[19,20] The cluster also most strongly expressed genes encoding gap junction connexins 43 and 45 (*GJA1* and *GJC1*, respectively; Figure 1B), which play key roles in fast conduction fibers,[21] and was characterized by several gene ontology (GO) terms related to conduction and signaling (Figure 1C). Taken together, these observations suggest that cluster 2 consisted of **Purkinje CMs**.

The second largest ventricular CM cluster (cluster 1) was associated with GO terms related to glycolysis[22] and response to hypoxia,[23] indicating high energy production. Moreover, this cluster strongly differentially

expressed the gene *HEY2* (p_val_adj 2.5 × $10^{-27}$) (Figures S2A and S2B), which is a downstream effector of NOTCH signaling that plays a pivotal role in the maturation of **compact CMs**.[24] *HEY2* represses atrial and trabecular gene expression of *TBX5*,[25] *NPPA*, and *GJA5* (encoding connexin 40). Thus, the cells in this cluster have characteristics of **compact CMs**.

The largest ventricular CM cluster (cluster 0) contained about a third of the ventricular CMs (Figure 1B). GO characteristics (Figure 1C) included more pronounced contractile- and membrane-related terms than for terms related to compact CMs. Several contractile-related genes were enriched (Figures S2A and S2B), such as *MYL2*, *TNNI3*, and *MYL3*. *HOPX*, a transcription factor involved in CM maturation[26] was also highly expressed (p_val_adj 6.3 × $10^{-26}$). Thus, cells in this cluster have characteristics of **trabecular CMs**.

The smallest ventricular CM cluster (cluster 7) was associated with few L-R interactions and weak expression of both *MYH7* and connexin expression (Figure 1B). Unique GO terms were related to mesenchyme development and both extracellular and cytoskeleton traits (Figure 1C). Fractions of the cells in G2M and S phases were high: 30.4% and 21.7%, respectively.

Highly differentially expressed genes (Figures S2A and S2B) included *LGALS1* (p_val_adj 1.2 × $10^{-7}$), *PLAC9* (p_val_adj 5.2 × $10^{-13}$), *ACTG1* (p_val_adj 4.4 × $10^{-12}$), and *S100A11* (p_val_adj 2.9 × $10^{-14}$). *LGALS1* encodes a beta-galactosidase-binding protein implicated in cell–matrix interactions, and colocalizes with intracellular sarcomeric actin.[27] *PLAC9* encodes a glycoprotein implicated in the extracellular matrix network.[28] *ACTG1* encodes a major constituent protein of the contractile apparatus; and *S100A11* encodes a calcium-binding protein. These properties suggest that cells in this cluster are cardiomyofibroblasts, developing mainly in the outflow tract (**OFT CMs**), where ventricular muscle as well as semilunar valves and the great arteries develop.[29–31]

The majority of the cells in the third smallest ventricular CM were in G2M phase (Figure 1B) and their GO terms (Figure 1C) were related to G2M phase and mitosis. In addition, the high DE of genes *PTTG1* (p_val_adj 3.9 × $10^{-35}$) and *TUBA1B* (p_val_adj 9.7 × $10^{-29}$) indicates pronounced G2M cell cycle activity. Thus, this cluster has characteristics of **high G2M CMs.**

Contrarywise, the second smallest ventricular CM (cluster 6) presents a low fraction of cells in G2M phase and 68% of the significant DE genes were mRNA of ribosomal proteins (Figure 1B). Of the remaining 24 DE genes, 18 have been documented in human vesicles including exosomes.[32] Associated GO terms are indicative of high ER activities. The gene *YBX1* was highly differentially expressed (p_val_adj 8.8 × $10^{-16}$) (Figures S2A and S2B) and is involved in recognition of RNA molecules and exosomal transport of microRNAs (miRNAs),[33–35] in accordance with GO characteristics indicating protein targeting to ER. Thus, this cluster has characteristics of **exosome-related CMs.**

Gene expression and cell cycle phase scores were highly variable both between and within the ventricular CM clusters (Figures S2C and S2D). All ventricular cell types included some in the G2M phase. Mitochondrial gene expression was also highly variable. It was low in OFT CMs, but there were also distinct fractions of cells with low expression in compact, trabecular, and exosome-enriched CMs (Figure S2C). These weakly expressing cells were localized in the HDCA dataset to the *MYOZ2*-enriched CM cluster, while the remaining cells were localized to the ventricular CM cluster. Overall, the weakly expressing cells (16% of the total) had lower numbers of expressed genes and transcripts and weaker mitochondrial gene expression than other cells, but a higher fraction in the G2M phase (26% vs 14%; $p < 0.001$ according to the chi-square test).

As additional validation, the CM scRNA-seq clusters were deconvoluted onto ST cardiac morphology maps, where four of the six ventricular CM clusters were anchored to relevant anatomic structures of the heart (Figures 1D and S3). Compact CMs were mainly located close to the epicardium of both ventricles and in the septum, while trabecular CMs were located in the inner parts of both ventricles. Purkinje fiber-related CMs were localized to the distal-central part of the right and left ventricles, while OFT CMs were mainly located in the outflow tract. Exosome-related and high-G2M CMs were diffusely distributed in the ventricles.

## Atrial cardiomyocyte types

As there were too few **SAN CMs** to identify by the clustering algorithm, they were detected using a supervised approach as cells coexpressing *TBX18*, *SHOX2*, and *HCN4*.[36–38] In the map generated by UMAP

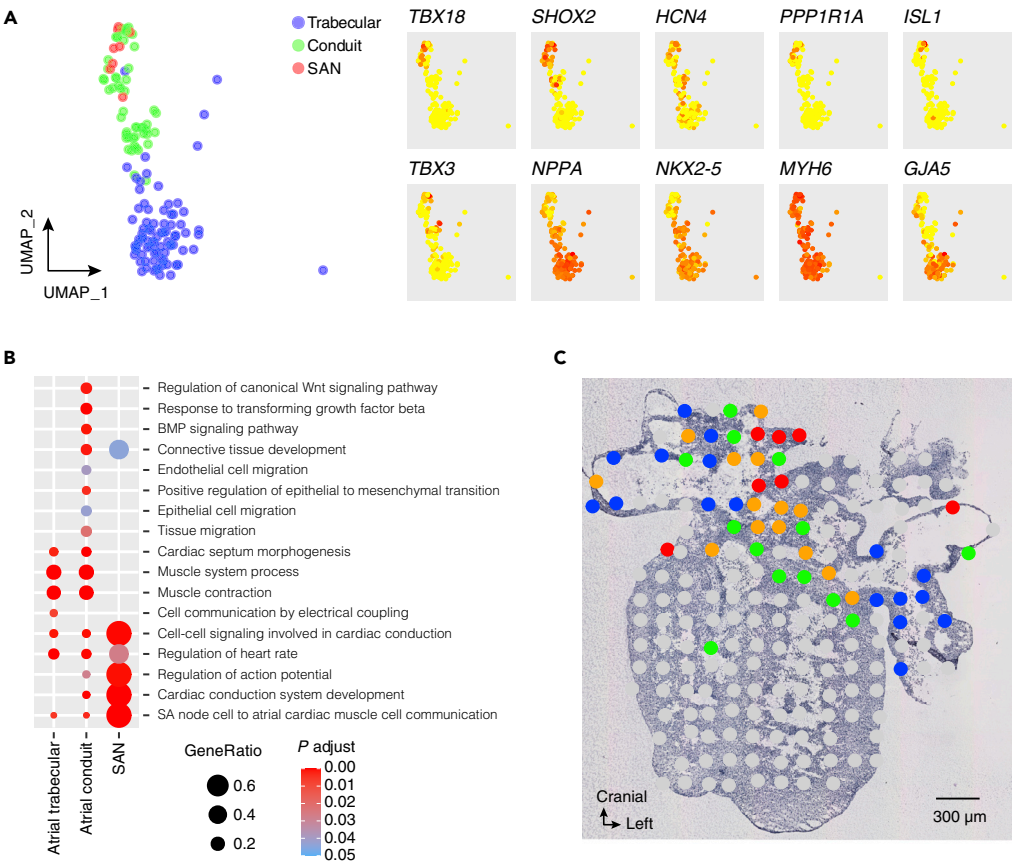


**Figure 2. Atrial CM subtype properties**

(A) Two-dimensional UMAP of atrial trabecular, conduit, and SAN CMs and heatmaps of relevant genes.

(B) GO characteristics: biological processes.

(C) Deconvolution of atrial CM types and their locations on an ST map.

analysis (Figure 2A), showing the two atrial clusters (clusters 3 and 5), SAN CMs (i.e., 8 cells in total) are located at the end of atrial cluster 5. Figure 2A also shows the expression sites of 10 markers related to atrial function. TBX18 is specifically at the upper end of cluster 5, i.e. in the SAN CM area, while *SHOX2* expression was more prominently and widely dispersed within cluster 5 (Figure S4). At this developmental stage expression of *SHOX2*, a growth factor of mesodermal origin is restricted to the right atrial conduit area[19,39,40] and left atrial conduit area around the pulmonary vein orifices. Our results are in agreement with previous findings where *SHOX2*, in concert with the proepicardial and mesenchymal derived transcription factor *TBX18*,[41] is related to the development of SAN pacemaker CMs and associated decreased expression of the myocardial contractile gene program's expression. As shown in Figure 2A, this involves the early cardiac transcription factor *NKX2-5* (expressed less strongly in cluster 5 than cluster 3, and in SAN less strongly than in cluster 5 (CMs: $p < 0.008$ and $<0.003$, respectively), and increased expression ($p < 0.0001$) of conduction-associated transcription factor *TBX3*. In parallel, *NPPA* was expressed less strongly in cluster 5 than in cluster 3 and less strongly in SAN than in cluster 5 (CMs: $p < 0.0001$ and $<0.004$, respectively) and the connexin 40-encoding gene *GJA5* was expressed less strongly in cluster 5 than in cluster 3: $p < 0.0001$. Such adaptations might prevent SAN CMs from becoming contracting fast-conducting atrial CMs.[38,42] In addition, expression of *PPP1R1A*, gene that encodes a cytoplasmic protein phosphatase inhibitor that modulates a clock mechanism that impacts on intrinsic automaticity of the SAN pacemaker cells,[43] was higher ($p < 0.0001$) in the SAN than in cluster 5.

The two atrial CM clusters (clusters 3 and 5) were similar in muscular contractility GO terms (Figure 2B), but only the smaller cluster (5) expressed epithelial cell migration, epithelial-to-mesenchymal transition, endothelial cell proliferation, bone morphogenetic protein (BMP), and canonical WNT signaling pathways.

These differences suggest that the larger cluster (3) is related to the primordial atria, developing mainly into the trabeculated atrial appendages (**atrial trabecular CMs**) while cluster 5 is related to the central smooth-walled part of the atria developing from the epicardium and mesenchyme and large veins, including the pulmonary veins[8,9,30] (**atrial conduit CMs**). The GO terms of SAN CMs (Figure 2B) were related to conduction, regulation of action potential, and heart rate. As additional validation, Figures 2C and S3 show that SAN CMs were localized to the upper part of the right atrium and the conduit atrial CMs mainly localized to the central part of the atria, while the trabecular atrial CMs were located more peripherally in the atria. Signals of both trabecular and conduit CMs were detected in several central spots. This was presumably because each spot in the spatial grid of a microdissected transcriptomic map may represent 20–30 cells, which could, of course, include different colocalized cell types.

## Spatial colocalization of different cell types

The interactions between different cell types during organ development are highly important. By deconvoluting non-cardiomyocyte (non-CM) single-cell clusters from the *HDCA* (Figure S1A) onto ST spots, we can visualize colocalized cell types and thus obtain indications of the key cells and their interactions in local development. Figure 3A shows the ST spots in the OFT region of one tissue section that contained OFT CMs and Figure 3B shows the fraction of spots with non-CMs colocalized to these OFT CM spots. Fractions of epicardium-derived cells, fibroblast-like cells related to larger and smaller vasculature, fibroblast-like smooth muscle cells and cardiac skeleton cells, endothelial, and Schwann progenitor cells were all high in these spots. In ST spots with unique atrial conduit CMs (Figure 3B), a similar composition of cell types was observed although also epicardial cells were present. Fractions of non-CM cell types were lower. This indicates that CMs may play a less prominent role in the OFT region (where major developmental events include septation and formation of the aorta, pulmonary artery, and semilunar valves) than they play in the atria, where muscle formation is the major developmental event.

## Ligand–receptor crosstalk

The number of L-R interactions[44] between different CM types was low, with practically no integrin interactions (Figure S5A). By contrast, interactions between ventricular CM and non-CM cells (Figure S5A) were pronounced and highest for the regionally located compact, trabecular, and Purkinje-related CMs, which also had the highest number of integrin interactions, indicating the importance of connective tissue and vascular structures in cardiac development and in CM development and anchoring.

In OFT CM spots, the majority of detected L-R interactions (Figure 3C) were between fibroblast-like cells related to vascular development, endothelial cells, epicardium-derived cells, and Schwann progenitor cells. Crosstalk between OFT CMs and these cell types was comparatively weak, possibly because CMs play a minor role in OFT development, which involves septation and valve formation. Of 27 OFT CM interactions (Figure 3D) identified, 12 (44%) involved integrins with specific L-R interactions from and toward the OFT CMs. Of non-integrins, OFT CMs expressed placental growth factor, which acts at several receptors (FLT1, NRP1, and NRP2) stimulating endothelial growth and angiogenesis. More non-CM ligands acted on OFT CMs than vice versa.

The complexity of L-R interactions is exemplified by those involving epidermal growth factor receptor (EGFR), which participates in crosstalk between various non-CM cell types and OFT CMs depending on the ligand involved (NRG1, TGFB1, MIF, or GRN). This is consistent with EGFR's role in the development of bicuspid valves and vascular structures.[45,46] Other agents involved in the interactions included BMP, LRP1 (low-density lipoprotein receptor), and TNFR. BMP is a member of the TGF-beta superfamily and, along with NOTCH signaling, regulates CM proliferation.[47,48] LRP1 affects cardiomyocyte lipid uptake, while TNFR activation may be involved in apoptosis, and has been described as recruiting cardiac progenitor cells[49] and stimulating OFT CMs. LGAL, NCAM1, and ESAM are ligands involved in cell-to-cell and cell-to-matrix interactions. Thus, the identified L-R crosstalk suggests aspects of the development of OFT CMs in their environment.

As neural crest derivatives are important for the development of the outflow tract in septation, L-R interactions between Schwann progenitor cells, the most prominent neural crest derivative in the OFT (Figure 3B), and colocalized cell types were explored (Figure S5B). Of the 153 detected L-R interactions, 92 (60%) involved integrins. Importantly, Schwann progenitor cells crosstalked via an array of cytokines with endothelium and with another array of cytokines with epicardium-derived cells, fibroblasts, and smooth muscle.

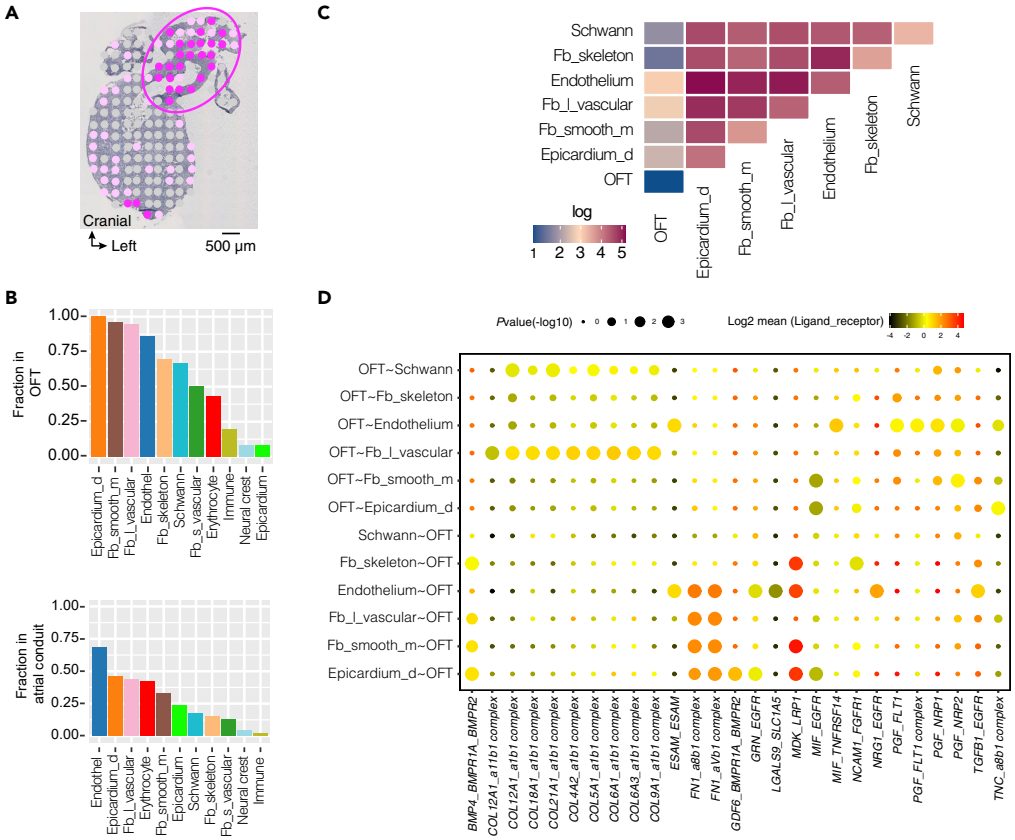


**Figure 3. Colocalized non-CM cell types with OFT CMs and relative ligand-receptor crosstalk**

(A) ST spots with projected OFT CMs in the OFT region (ellipse) in heart section 115.

(B) Fraction of spots expressing non-CM cell types deconvoluted from scRNA-seq clusters described in Figure S1 for spots expressing (above) OFT CMs and (below) conduit atrial CMs.

(C) Heatmap showing numbers of L-R interactions between OFT CMs and non-CMs.

(D) Specific highly expressed L-R crosstalk between OFT CMs and colocalized non-CM cell types. Abbreviations of non-cardiomyocyte cell types: Epicardium-d: Epicardium-derived, Fb_l_vascular: Fibroblast-like (larger vascular development), Fb_smooth_m: Fibroblast-like smooth muscle cells, Schwann: Schwann progenitor cells, Fb_skeleton: Fibroblast-like (cardiac skeleton). "Log2mean (ligand-receptor)" indicates the ratio between the mean expression level in interacting molecule in cluster 1 divided with the mean expression level in interacting molecule in cluster 2. "p value(-log10)" refers to the enrichment of the interacting ligand-receptor pair in each of the interacting pairs of cell types.

Moreover, also ephrins, NOTCH, TGF-beta, and tyrosine kinase interactions were active between Schwann progenitor cells and the other cell types.

The exosome-related CMs were interspersed throughout the ventricular muscle (Figure 1D). Only 32 detected L-R interactions of these cells were significant, of which 11 (34%) involved integrins (Figure S5C). Integrin ligands were only expressed at exosome-related CMs, indicating unidirectional binding to non-CMs. Both FGF and VEGF ligands acted through various receptors at colocalized cells, as did TNF, BMP, NPPA, and tyrosine kinase AXL, affecting the smooth muscle, fibroblasts, and endothelium. Extracellular instructive signals affecting exosome-related CMs included L-R crosstalk with the nodal morphogen TGF-beta pair LEFTY2_TDGF1[50–52] and CD47_SIRPA, suggesting that these CMs are at an early stage of development. SIPRA is a cell surface receptor expressed at cardiomyocyte progenitors and early cardiomyocytes.[53,54]

## Sinoatrial node and conduit cardiomyocytes

Figure 3B shows that ST spots with atrial conduit CMs contained, with the addition of epicardial cells, similar non-CM cell types to spots with OFT CMs, although with smaller non-CM fractions, suggesting that the major cell type in these spots was conduit CMs.

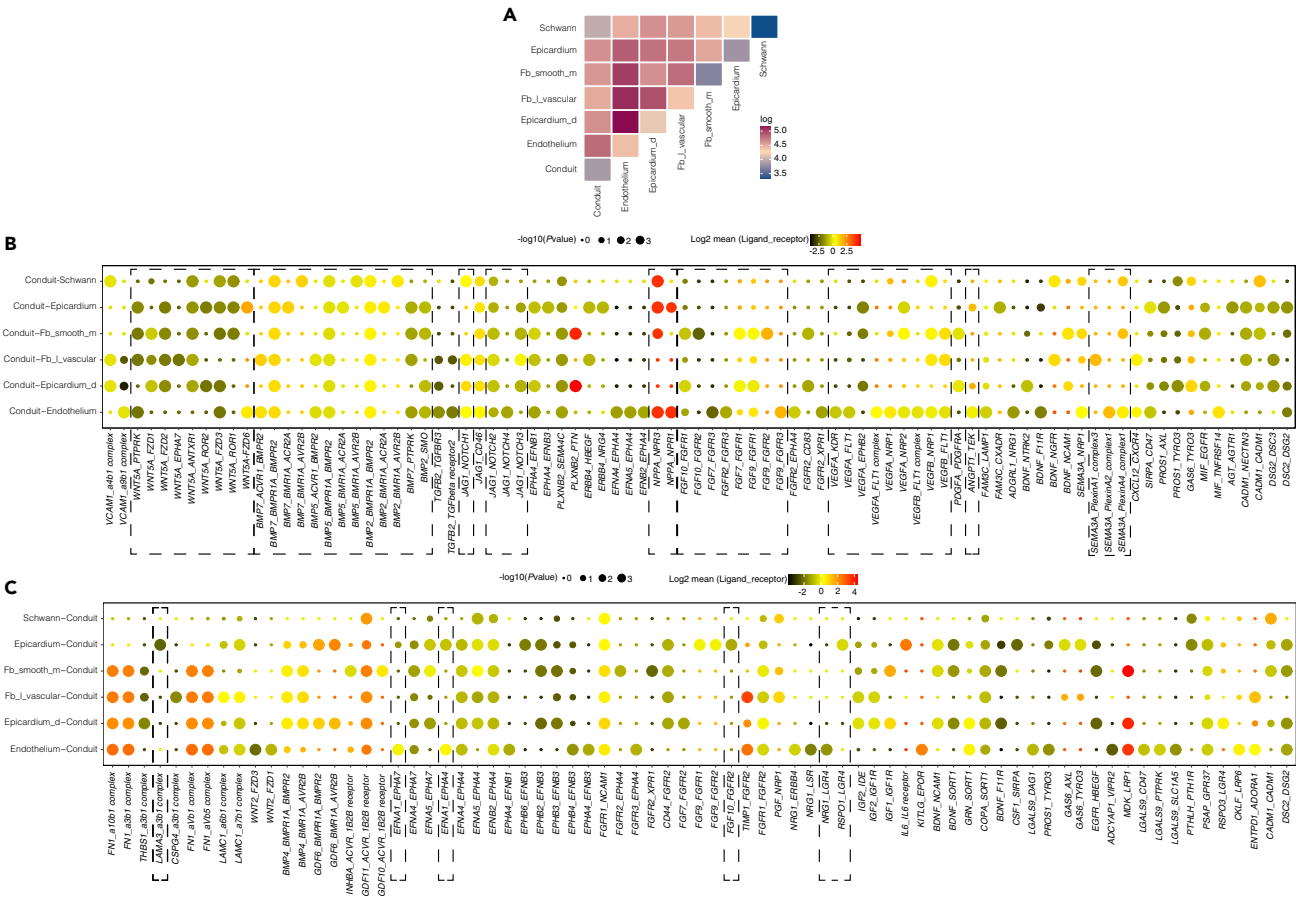


**Figure 4. Colocalized non-CM cell types with conduit CMs and relative ligand-receptor crosstalk**

(A) Heatmap showing numbers of L-R interactions between conduit atrial CM clusters and six non-CM clusters.

(B) Specific highly expressed L-R crosstalk between conduit and colocalized non-CMs.

(C) Specific highly expressed L-R crosstalk between colocalized non-CMs and conduit CMs. Abbreviations of non-cardiomyocyte cell types: Fb_l_vascular: Fibroblast-like (larger vascular development), Epicardium-d: Epicardium-derived, Fb_skeleton: Fibroblast-like (cardiac skeleton). Fb_smooth_m: Fibroblast-like smooth muscle cells, Fb_s_vascular: Fibroblast-like (smaller vascular development). "Log2mean (ligand-receptor)" indicates the ratio between the mean expression level in interacting molecule in cluster 1 divided with the mean expression level in interacting molecule in cluster 2. "p value(-log10)" refers to the enrichment of the interacting ligand-receptor pair in each of the interacting pairs of cell types.

We detected more L-R interactions of conduit CMs with non-CM cells (i.e., 226, including 72 integrin interactions) (Figure 4A) than those of OFT CMs (Figure 3C). For example, conduit CMs communicated with all the analyzed non-CM cell types via NOTCH, WNT, or BMP signaling pathways, which are fundamental during cardiac development[55] (Figure 4B). In addition, NPPA, fibroblast growth factors (FGFs), VEGFs, angiopoietin, and Semaphorin 3[56] ligands, which are known to promote vasculogenesis, interacted profoundly with endothelial cells from conduit CMs. Finally, conduit CMs had broad interactions with epicardial cells and endothelial cells (Figure 4A). In this respect, LAMA3, FGF10, EFNA1, and LGR4 (Figure 4C) have been implicated in epithelial-to-mesenchymal transition[57–60] that may, in the atrial wall of venous origin, contribute to its myocardialization.[41,61–64]

## DISCUSSION

The human embryonic heart at 6.5–7 PCW is in a dynamic phase, in which the left and right ventricles of the myocardium grow and the musculature of the proximal OFT is still developing.

Our results show that rates of cell division and RNA synthesis are high, but heterogeneous, in the main part of the ventricular CM population, and they have high heterogeneity in expression of mitochondrial genes and connexin 43 (a marker of the intercellular electrical connectedness between CMs). This heterogeneity is

consistent with previous findings that cell cycle gene expression downregulates sarcomeric and cytoskeletal markers, through location-specific signaling molecules that may influence the proliferation of colocalized cells.[65] We also detected extensive L-R crosstalk, with specific profiles, as exemplified for OFT, exosome-related and conduit atrium CMs, and Schwann progenitor cells.

In contrast to the located trabecular, compact, and Purkinje CMs, two CM types, exosome-related and high G2M CMs, have lower expressions of *MYH7*, connexins, and mitochondria and are dispersed throughout the spatial compartments. The small exosome-related CMs have a pronounced expression of mRNA of exosomal proteins. These CMs may warrant more attention in the development of exosome-based regeneration of CMs for therapeutic heart failure treatments.[66]

The OFT CMs differ from the compact and trabecular CMs, having a more fibroblast-like profile. The proximal OFT, conus of the right ventricle, and left ventricular OFT develop later than the compact and ventricular myocardium.[67] With respect to DE and GO characteristics, the OFT CMs expressed genes related to connective tissue development. There is some debate as to whether outflow myocardialization is based on the ingrowth of ventricular CMs or differentiation from mesenchyme, epicardium, and endocardium related to the OFT.[67] Our results suggest that the latter source may be important, at least in the hearts analyzed.

In conclusion, our combined analysis of single-cell and spatial transcriptomic analysis, as well as L-R crosstalk between spatially colocalized cell types, reveals a complex landscape of dynamic changes in the cellular composition, expression patterns, and functions of CMs in the early prenatal human heart. Our approach also provides a strategy to characterize further the combined and publicly available single-cell and spatial transcriptomics resources.

### Limitations of the study

The study is based on published datasets by Asp et al., 2019. Due to the scarcity of human prenatal material, these datasets are based on two hearts of similar post-conception age. Our hypothesis-generating results have been obtained by applying *in silico* methods. Further experimental validation would strengthen our findings.

## STAR★METHODS

Detailed methods are provided in the online version of this paper and include the following:

- KEY RESOURCES TABLE
- RESOURCE AVAILABILITY
  - Lead contact
  - Materials availability
  - Data and code availability
- EXPERIMENTAL MODEL AND SUBJECT DETAILS
- METHOD DETAILS
  - Data
  - scRNA-seq analysis
  - GO characterization
  - Cardiomyocyte cell type validation
  - L-R crosstalk
- QUANTIFICATION AND STATISTICAL ANALYSIS

## SUPPLEMENTAL INFORMATION

Supplemental information can be found online at https://doi.org/10.1016/j.isci.2022.105857.

## ACKNOWLEDGMENTS

This work was supported by the Swedish Research Council Formas grant 2017-01066 and Vetenskapsrådet grant 2020-04864 to S.G., the Erling-Persson Family Foundation, and the Knut and Alice Wallenberg Foundation. Å.B. was supported by the Knut and Wallenberg Foundation as part of the National Bioinformatics Infrastructure Sweden at SciLifeLab. We thank Yuvarani Masarapu for help with the GitHub repository.

## AUTHOR CONTRIBUTIONS

C.S. conceived and designed the study, analyzed the data, interpreted the results, wrote the manuscript, and designed the figures. E.W. performed tissue sectioning and guided histological annotations. A.M.B. assisted in biological interpretation. E.C. conceived the study and assisted in biological interpretation. K.A. created the artwork. L.L. analyzed the data and interpreted the results that contributed to the final manuscript. Å.B. assisted in bioinformatics analysis. S.G. conceived the study, guided data analysis, interpreted the results, wrote the manuscript, and designed the figures. All authors helped with manuscript preparation.

## DECLARATION OF INTERESTS

S.G. is scientific advisor to 10x Genomics, which holds IP rights to the ST technology, and holds 10x Genomics stock options.

## INCLUSION AND DIVERSITY

We support inclusive, diverse, and equitable conduct of research.

Received: March 10, 2022
Revised: July 19, 2022
Accepted: December 18, 2022
Published: January 20, 2023

## REFERENCES

1. Sylva, M., van den Hoff, M.J.B., and Moorman, A.F.M. (2014). Development of the human heart. Am. J. Med. Genet. *164A*, 1347–1371. https://doi.org/10.1002/ajmg.a.35896.

2. Samsa, L.A., Yang, B., and Liu, J. (2013). Embryonic cardiac chamber maturation: trabeculation, conduction, and cardiomyocyte proliferation. Am. J. Med. Genet. C Semin. Med. Genet. *163C*, 157–168. https://doi.org/10.1002/ajmg.c.31366.

3. Günthel, M., Barnett, P., and Christoffels, V.M. (2018). Development, proliferation, and growth of the mammalian heart. Mol. Ther. *26*, 1599–1609. https://doi.org/10.1016/j.ymthe.2018.05.022.

4. DeRuiter, M.C., Gittenberger-De Groot, A.C., Wenink, A.C., Poelmann, R.E., and Mentink, M.M. (1995). In normal development pulmonary veins are connected to the sinus venosus segment in the left atrium. Anat. Rec. *243*, 84–92. https://doi.org/10.1002/ar.1092430110.

5. Faber, J.W., Boukens, B.J., Oostra, R.-J., Moorman, A.F.M., Christoffels, V.M., and Jensen, B. (2019). Sinus venosus incorporation: contentious issues and operational criteria for developmental and evolutionary studies. J. Anat. *234*, 583–591. https://doi.org/10.1111/joa.12962.

6. Soufan, A.T., van den Hoff, M.J.B., Ruijter, J.M., de Boer, P.A.J., Hagoort, J., Webb, S., Anderson, R.H., and Moorman, A.F.M. (2004). Reconstruction of the patterns of gene expression in the developing mouse heart reveals an architectural arrangement that facilitates the understanding of atrial malformations and arrhythmias. Circ. Res. *95*, 1207–1215. https://doi.org/10.1161/01.RES.0000150852.04747.e1.

7. Steding, G., Jinwen, X., Seidl, W., Männer, J., and Xia, H. (1990). Developmental aspects of the sinus valves and the sinus venosus septum of the right atrium in human embryos. Anat. Embryol. *181*, 469–475. https://doi.org/10.1007/BF02433794.

8. Douglas, Y.L., Mahtab, E.A.F., Jongbloed, M.R.M., Uhrin, P., Zaujec, J., Binder, B.R., Schalij, M.J., Poelmann, R.E., Deruiter, M.C., and Gittenberger-de Groot, A.C. (2009). Pulmonary vein, dorsal atrial wall and atrial septum abnormalities in podoplanin knockout mice with disturbed posterior heart field contribution. Pediatr. Res. *65*, 27–32. https://doi.org/10.1203/PDR.0b013e31818bc11a.

9. Gallego, A., Durán, A.C., De Andrés, A.V., Navarro, P., and Muñoz-Chápuli, R. (1997). Anatomy and development of the sinoatrial valves in the dogfish (Scyliorhinus canicula). Anat. Rec. *248*, 224–232. https://doi.org/10.1002/(SICI)1097-0185(199706)248:2<224::AID-AR9>3.0.CO;2-S.

10. Salmén, F., Ståhl, P.L., Mollbrink, A., Navarro, J.F., Vickovic, S., Frisén, J., and Lundeberg, J. (2018). Barcoded solid-phase RNA capture for Spatial Transcriptomics profiling in mammalian tissue sections. Nat. Protoc. *13*, 2501–2534. https://doi.org/10.1038/s41596-018-0045-2.

11. Ståhl, P.L., Salmén, F., Vickovic, S., Lundmark, A., Navarro, J.F., Magnusson, J., Giacomello, S., Asp, M., Westholm, J.O., Huss, M., et al. (2016). Visualization and analysis of gene expression in tissue sections by spatial transcriptomics. Science *353*, 78–82. https://doi.org/10.1126/science.aaf2403.

12. Zheng, G.X.Y., Terry, J.M., Belgrader, P., Ryvkin, P., Bent, Z.W., Wilson, R., Ziraldo, S.B., Wheeler, T.D., McDermott, G.P., Zhu, J., et al. (2017). Massively parallel digital transcriptional profiling of single cells. Nat. Commun. *8*, 14049. https://doi.org/10.1038/ncomms14049.

13. Ke, R., Mignardi, M., Pacureanu, A., Svedlund, J., Botling, J., Wählby, C., and Nilsson, M. (2013). In situ sequencing for RNA analysis in preserved tissue and cells. Nat. Methods *10*, 857–860. https://doi.org/10.1038/nmeth.2563.

14. Qian, X., Harris, K.D., Hauling, T., Nicoloutsopoulos, D., Muñoz-Manchado, A.B., Skene, N., Hjerling-Leffler, J., and Nilsson, M. (2020). Probabilistic cell typing enables fine mapping of closely related cell types in situ. Nat. Methods *17*, 101–106. https://doi.org/10.1038/s41592-019-0631-4.

15. Becht, E., McInnes, L., Healy, J., Dutertre, C.-A., Kwok, I.W.H., Ng, L.G., Ginhoux, F., and Newell, E.W. (2018). Dimensionality reduction for visualizing single-cell data using UMAP. Nat. Biotechnol. *37*, 38–44. https://doi.org/10.1038/nbt.4314.

16. Asp, M., Giacomello, S., Larsson, L., Wu, C., Fürth, D., Qian, X., Wärdell, E., Custodio, J., Reimegård, J., Salmén, F., et al. (2019). A spatiotemporal organ-wide gene expression and cell atlas of the developing human heart. Cell *179*, 1647–1660.e19. https://doi.org/10.1016/j.cell.2019.11.025.

17. Kolanowski, T.J., Busek, M., Schubert, M., Dmitrieva, A., Binnewerg, B., Pöche, J., Fisher, K., Schmieder, F., Grünzner, S., Hansen, S., et al. (2020). Enhanced structural maturation of human induced pluripotent stem cell-derived cardiomyocytes under a controlled microenvironment in a microfluidic system. Acta Biomater. *102*, 273–286. https://doi.org/10.1016/j.actbio.2019.11.044.

18. Saheli, M., Pirhajati Mahabadi, V., Mesbah-Namin, S.A., Seifalian, A., and Bagheri-

Hosseinabadi, Z. (2020). DNA methyltransferase inhibitor 5-azacytidine in high dose promotes ultrastructural maturation of cardiomyocyte. Stem Cell Invest. *7*, 22. https://doi.org/10.21037/sci-2020-007.

19. Hu, W., Xin, Y., Zhang, L., Hu, J., Sun, Y., and Zhao, Y. (2018). Iroquois Homeodomain transcription factors in ventricular conduction system and arrhythmia. Int. J. Med. Sci. *15*, 808–815. https://doi.org/10.7150/ijms.25140.

20. Kim, K.-H., Rosen, A., Hussein, S.M.I., Puviindran, V., Korogyi, A.S., Chiarello, C., Nagy, A., Hui, C.-C., and Backx, P.H. (2016). Irx3 is required for postnatal maturation of the mouse ventricular conduction system. Sci. Rep. *6*, 19197. https://doi.org/10.1038/srep19197.

21. Boukens, B.J., Sylva, M., de Gier-de Vries, C., Remme, C.A., Bezzina, C.R., Christoffels, V.M., and Coronel, R. (2013). Reduced sodium channel function unmasks residual embryonic slow conduction in the adult right ventricular outflow tract. Circ. Res. *113*, 137–141. https://doi.org/10.1161/CIRCRESAHA.113.301565.

22. Graham, N., and Huang, G.N. (2021). Endocrine influence on cardiac metabolism in development and regeneration. Endocrinology *162*, bqab081. https://doi.org/10.1210/endocr/bqab081.

23. Meng, X., Zhang, P., and Zhang, L. (2020). Fetal hypoxia impacts on proliferation and differentiation of sca-1+ cardiac progenitor cells and maturation of cardiomyocytes: a role of MicroRNA-210. Genes *11*, E328. https://doi.org/10.3390/genes11030328.

24. Firulli, B.A., George, R.M., Harkin, J., Toolan, K.P., Gao, H., Liu, Y., Zhang, W., Field, L.J., Liu, Y., Shou, W., et al. (2020). HAND1 loss-of-function within the embryonic myocardium reveals survivable congenital cardiac defects and adult heart failure. Cardiovasc. Res. *116*, 605–618. https://doi.org/10.1093/cvr/cvz182.

25. Steimle, J.D., and Moskowitz, I.P. (2017). TBX5: a key regulator of heart development. Curr. Top. Dev. Biol. *122*, 195–221. https://doi.org/10.1016/bs.ctdb.2016.08.008.

26. Friedman, C.E., Nguyen, Q., Lukowski, S.W., Helfer, A., Chiu, H.S., Miklas, J., Levy, S., Suo, S., Han, J.-D.J., Osteil, P., et al. (2018). Single-cell transcriptomic analysis of cardiac differentiation from human PSCs reveals HOPX-dependent cardiomyocyte maturation. Cell Stem Cell *23*, 586–598.e8. https://doi.org/10.1016/j.stem.2018.09.009.

27. Dias-Baruffi, M., Stowell, S.R., Song, S.-C., Arthur, C.M., Cho, M., Rodrigues, L.C., Montes, M.A.B., Rossi, M.A., James, J.A., McEver, R.P., and Cummings, R.D. (2010). Differential expression of immunomodulatory galectin-1 in peripheral leukocytes and adult tissues and its cytosolic organization in striated muscle. Glycobiology *20*, 507–520. https://doi.org/10.1093/glycob/cwp203.

28. Cui, Y., Zheng, Y., Liu, X., Yan, L., Fan, X., Yong, J., Hu, Y., Dong, J., Li, Q., Wu, X., et al. (2019). Single-cell transcriptome analysis maps the developmental track of the human heart. Cell Rep. *26*, 1934–1950.e5. https://doi.org/10.1016/j.celrep.2019.01.079.

29. Boukens, B.J.D., Christoffels, V.M., Coronel, R., and Moorman, A.F.M. (2009). Developmental basis for electrophysiological heterogeneity in the ventricular and outflow tract myocardium as a substrate for life-threatening ventricular arrhythmias. Circ. Res. *104*, 19–31. https://doi.org/10.1161/CIRCRESAHA.108.188698.

30. van den Hoff, M.J., Kruithof, B.P., Moorman, A.F., Markwald, R.R., and Wessels, A. (2001). formation of myocardium after the initial development of the linear heart tube. Dev. Biol. *240*, 61–76. https://doi.org/10.1006/dbio.2001.0449.

31. Sahara, M., Santoro, F., Sohlmér, J., Zhou, C., Witman, N., Leung, C.Y., Mononen, M., Bylund, K., Gruber, P., and Chien, K.R. (2019). Population and single-cell analysis of human cardiogenesis reveals unique LGR5 ventricular progenitors in embryonic outflow tract. Dev. Cell *48*, 475–490.e7. https://doi.org/10.1016/j.devcel.2019.01.005.

32. Pathan, M., Fonseka, P., Chitti, S.V., Kang, T., Sanwlani, R., Van Deun, J., Hendrix, A., and Mathivanan, S. (2019). Vesiclepedia 2019: a compendium of RNA, proteins, lipids and metabolites in extracellular vesicles. Nucleic Acids Res. *47*, D516–D519. https://doi.org/10.1093/nar/gky1029.

33. Lin, F., Zeng, Z., Song, Y., Li, L., Wu, Z., Zhang, X., Li, Z., Ke, X., and Hu, X. (2019). YBX-1 mediated sorting of miR-133 into hypoxia/reoxygenation-induced EPC-derived exosomes to increase fibroblast angiogenesis and MEndoT. Stem Cell Res. Ther. *10*, 263. https://doi.org/10.1186/s13287-019-1377-8.

34. Shurtleff, M.J., Yao, J., Qin, Y., Nottingham, R.M., Temoche-Diaz, M.M., Schekman, R., and Lambowitz, A.M. (2017). Broad role for YBX1 in defining the small noncoding RNA composition of exosomes. Proc. Natl. Acad. Sci. USA *114*, E8987–E8995. https://doi.org/10.1073/pnas.1712108114.

35. Suresh, P.S., Tsutsumi, R., and Venkatesh, T. (2018). YBX1 at the crossroads of non-coding transcriptome, exosomal, and cytoplasmic granular signaling. Eur. J. Cell Biol. *97*, 163–167. https://doi.org/10.1016/j.ejcb.2018.02.003.

36. Easterling, M., Rossi, S., Mazzella, A.J., and Bressan, M. (2021). Assembly of the cardiac pacemaking complex: electrogenic principles of sinoatrial node morphogenesis. J. Cardiovasc. Dev. Dis. *8*, 40. https://doi.org/10.3390/jcdd8040040.

37. Liang, X., Evans, S.M., and Sun, Y. (2017). Development of the cardiac pacemaker. Cell. Mol. Life Sci. *74*, 1247–1259. https://doi.org/10.1007/s00018-016-2400-1.

38. Wiese, C., Grieskamp, T., Airik, R., Mommersteeg, M.T.M., Gardiwal, A., de Gier-de Vries, C., Schuster-Gossler, K., Moorman, A.F.M., Kispert, A., and Christoffels, V.M. (2009). Formation of the sinus node head and differentiation of sinus node myocardium are independently regulated by Tbx18 and Tbx3. Circ. Res. *104*, 388–397. https://doi.org/10.1161/CIRCRESAHA.108.187062.

39. Espinoza-Lewis, R.A., Yu, L., He, F., Liu, H., Tang, R., Shi, J., Sun, X., Martin, J.F., Wang, D., Yang, J., and Chen, Y. (2009). Shox2 is essential for the differentiation of cardiac pacemaker cells by repressing Nkx2-5. Dev. Biol. *327*, 376–385. https://doi.org/10.1016/j.ydbio.2008.12.028.

40. Liu, H., Espinoza-Lewis, R.A., Chen, C., Hu, X., Zhang, Y., and Chen, Y. (2012). The role of Shox2 in SAN development and function. Pediatr. Cardiol. *33*, 882–889. https://doi.org/10.1007/s00246-012-0179-x.

41. Cai, C.-L., Martin, J.C., Sun, Y., Cui, L., Wang, L., Ouyang, K., Yang, L., Bu, L., Liang, X., Zhang, X., et al. (2008). A myocardial lineage derives from Tbx18 epicardial cells. Nature *454*, 104–108. https://doi.org/10.1038/nature06969.

42. van Eif, V.W.W., Stefanovic, S., van Duijvenboden, K., Bakker, M., Wakker, V., de Gier-de Vries, C., Zaffran, S., Verkerk, A.O., Boukens, B.J., and Christoffels, V.M. (2019). Transcriptome analysis of mouse and human sinoatrial node cells reveals a conserved genetic program. Development *146*, dev173161. https://doi.org/10.1242/dev.173161.

43. Sirenko, S.T., Zahanich, I., Li, Y., Lukyanenko, Y.O., Lyashkov, A.E., Ziman, B.D., Tarasov, K.V., Younes, A., Riordon, D.R., Tarasova, Y.S., et al. (2021). Phosphoprotein phosphatase 1 but not 2A activity modulates coupled-clock mechanisms to impact on intrinsic automaticity of sinoatrial nodal pacemaker cells. Cells *10*, 3106. https://doi.org/10.3390/cells10113106.

44. Efremova, M., Vento-Tormo, M., Teichmann, S.A., and Vento-Tormo, R. (2020). CellPhoneDB: inferring cell-cell communication from combined expression of multi-subunit ligand-receptor complexes. Nat. Protoc. *15*, 1484–1506. https://doi.org/10.1038/s41596-020-0292-x.

45. Makki, N., Thiel, K.W., and Miller, F.J. (2013). The epidermal growth factor receptor and its ligands in cardiovascular disease. Int. J. Mol. Sci. *14*, 20597–20613. https://doi.org/10.3390/ijms141020597.

46. Schroeder, J.A., Jackson, L.F., Lee, D.C., and Camenisch, T.D. (2003). Form and function of developing heart valves: coordination by extracellular matrix and growth factor signaling. J. Mol. Med. *81*, 392–403. https://doi.org/10.1007/s00109-003-0456-5.

47. D'Amato, G., Luxán, G., and de la Pompa, J.L. (2016). Notch signalling in ventricular chamber development and cardiomyopathy. FEBS J. *283*, 4223–4237. https://doi.org/10.1111/febs.13773.

48. Sorensen, D.W., and van Berlo, J.H. (2020). The role of TGF-β signaling in cardiomyocyte proliferation. Curr. Heart Fail. Rep. *17*, 225–233. https://doi.org/10.1007/s11897-020-00470-2.

49. Allukian, M., Xu, J., Morris, M., Caskey, R., Dorsett-Martin, W., Plappert, T., Griswold, M., Gorman, J.H., Gorman, R.C., and Liechty, K.W. (2013). Mammalian cardiac regeneration after fetal myocardial infarction requires cardiac progenitor cell recruitment. Ann. Thorac. Surg. *96*, 163–170. https://doi.org/10.1016/j.athoracsur.2013.04.005.

50. Barnes, R.M., and Black, B.L. (2016). Nodal signaling and congenital heart defects. In Etiology and Morphogenesis of Congenital Heart Disease: From Gene Function and Cellular Interaction to Morphology, T. Nakanishi, R.R. Markwald, H.S. Baldwin, B.B. Keller, D. Srivastava, and H. Yamagishi, eds. (Springer).

51. Behrens, A.N., Ren, Y., Ferdous, A., Garry, D.J., and Martin, C.M. (2012). Nkx2-5 regulates Tdgf1 (cripto) early during cardiac development. J clin exp cardiolog. J. Clin. Exp. Cardiol. *11*, 1–4. https://doi.org/10.4172/2155-9880.S11-003.

52. Noseda, M., Peterkin, T., Simões, F.C., Patient, R., and Schneider, M.D. (2011). Cardiopoietic factors: extracellular signals for cardiac lineage commitment. Circ. Res. *108*, 129–152. https://doi.org/10.1161/CIRCRESAHA.110.223792.

53. Dubois, N.C., Craft, A.M., Sharma, P., Elliott, D.A., Stanley, E.G., Elefanty, A.G., Gramolini, A., and Keller, G. (2011). SIRPA is a specific cell-surface marker for isolating cardiomyocytes derived from human pluripotent stem cells. Nat. Biotechnol. *29*, 1011–1018. https://doi.org/10.1038/nbt.2005.

54. Skelton, R.J.P., Costa, M., Anderson, D.J., Bruveris, F., Finnin, B.W., Koutsis, K., Arasaratnam, D., White, A.J., Rafii, A., Ng, E.S., et al. (2014). SIRPA, VCAM1 and CD34 identify discrete lineages during early human cardiovascular development. Stem Cell Res. *13*, 172–179. https://doi.org/10.1016/j.scr.2014.04.016.

55. MacGrogan, D., Münch, J., and de la Pompa, J.L. (2018). Notch and interacting signalling pathways in cardiac development, disease, and regeneration. Nat. Rev. Cardiol. *15*, 685–704. https://doi.org/10.1038/s41569-018-0100-2.

56. Valdembri, D., Regano, D., Maione, F., Giraudo, E., and Serini, G. (2016). Class 3 semaphorins in cardiovascular development. Cell Adhes. Migrat. *10*, 641–651. https://doi.org/10.1080/19336918.2016.1212805.

57. Huang, C., and Chen, J. (2021). Laminin-332 mediates proliferation, apoptosis, invasion, migration and epithelial-to-mesenchymal transition in pancreatic ductal adenocarcinoma. Mol. Med. Rep. *23*, 11. https://doi.org/10.3892/mmr.2020.11649.

58. Itoh, N. (2016). FGF10: a multifunctional mesenchymal-epithelial signaling growth factor in development, health, and disease. Cytokine Growth Factor Rev. *28*, 63–69. https://doi.org/10.1016/j.cytogfr.2015.10.001.

59. Frieden, L.A., Townsend, T.A., Vaught, D.B., Delaughter, D.M., Hwang, Y., Barnett, J.V., and Chen, J. (2010). Regulation of heart valve morphogenesis by Eph receptor ligand, ephrin-A1. Dev. Dynam. *239*, 3226–3234. https://doi.org/10.1002/dvdy.22458.

60. Zhang, H., Liang, F., Yue, J., Liu, P., Wang, J., Wang, Z., Li, H., Cheng, D., Du, J., Zhang, K., and Du, P. (2020). MicroRNA-137 regulates hypoxia-mediated migration and epithelial-mesenchymal transition in prostate cancer by targeting LGR4 via the EGFR/ERK signaling pathway. Int. J. Oncol. *57*, 540–549. https://doi.org/10.3892/ijo.2020.5064.

61. Greulich, F., Rudat, C., and Kispert, A. (2011). Mechanisms of T-box gene function in the developing heart. Cardiovasc. Res. *91*, 212–222. https://doi.org/10.1093/cvr/cvr112.

62. Singh, M., and Epstein, J. (2013). Epicardial lineages and cardiac repair. J. Dev. Biol. *1*, 141–158. https://doi.org/10.3390/jdb1020141.

63. Zhou, B., Ma, Q., Rajagopal, S., Wu, S.M., Domian, I., Rivera-Feliciano, J., Jiang, D., von Gise, A., Ikeda, S., Chien, K.R., and Pu, W.T. (2008). Epicardial progenitors contribute to the cardiomyocyte lineage in the developing heart. Nature *454*, 109–113. https://doi.org/10.1038/nature07060.

64. Marco Salas, S., Yuan, X., Sylven, C., Nilsson, M., Wählby, C., and Partel, G. (2022). De novo spatiotemporal modelling of cell-type signatures in the developmental human heart using graph convolutional neural networks. PLoS Comput. Biol. *18*, e1010366. https://doi.org/10.1371/journal.pcbi.1010366.

65. Li, G., Tian, L., Goodyer, W., Kort, E.J., Buikema, J.W., Xu, A., Wu, J., Jovinge, S., and Wu, S.M. (2019). Single cell expression analysis reveals anatomical and cell cycle-dependent transcriptional shifts during heart development. Development *146*, dev173476. https://doi.org/10.1242/dev.173476.

66. Barile, L., Moccetti, T., Marbán, E., and Vassalli, G. (2017). Roles of exosomes in cardioprotection. Eur. Heart J. *38*, 1372–1379. https://doi.org/10.1093/eurheartj/ehw304.

67. van den Hoff, M.J.B., and Wessels, A. (2020). Muscularization of the mesenchymal outlet septum during cardiac development. J. Cardiovasc. Dev. Dis. *7*, E51. https://doi.org/10.3390/jcdd7040051.

68. Butler, A., Hoffman, P., Smibert, P., Papalexi, E., and Satija, R. (2018). Integrating single-cell transcriptomic data across different conditions, technologies, and species. Nat. Biotechnol. *36*, 411–420. https://doi.org/10.1038/nbt.4096.

69. Andersson, A., Bergenstråhle, J., Asp, M., Bergenstråhle, L., Jurek, A., Fernández Navarro, J., and Lundeberg, J. (2020). Single-cell and spatial transcriptomics enables probabilistic inference of cell type topography. Commun. Biol. *3*, 565. https://doi.org/10.1038/s42003-020-01247-y.

70. Yu, G., Wang, L.-G., Han, Y., and He, Q.-Y. (2012). clusterProfiler: an R package for comparing biological themes among gene clusters. OMICS *16*, 284–287. https://doi.org/10.1089/omi.2011.0118.

71. Aibar, S., González-Blas, C.B., Moerman, T., Huynh-Thu, V.A., Imrichova, H., Hulselmans, G., Rambow, F., Marine, J.-C., Geurts, P., Aerts, J., et al. (2017). SCENIC: single-cell regulatory network inference and clustering. Nat. Methods *14*, 1083–1086. https://doi.org/10.1038/nmeth.4463.

# STAR★METHODS

## KEY RESOURCES TABLE

| REAGENT or RESOURCE | SOURCE | IDENTIFIER |
|---|---|---|
| Deposited data | | |
| Single-cell sequencing and spatial transcriptomic data | Asp et al.[16] | https://doi.org/10.17632/mbvhhf8m62.2 |
| Background ST maps grobs data | This paper | https://doi.org/10.17632/xgs5yf9zch.1 |
| Software and algorithms | | |
| Cardiomyocytes | This paper | https://github.com/giacomellolab/Human-Prenatal-Cardiomyocytes |
| CellPhoneDB | Efremova et al.[44] | https://github.com/Teichlab/cellphonedb |
| clusterProfiler | Yu et al.[70] | https://github.com/dalloliogm/clusterProfiler |
| SCENIC | Aibar et al.[71] | https://github.com/aertslab/pySCENIC |
| Seurat | Butler et al.[68] | https://github.com/satijalab/seurat |
| Stereoscope | Andersson et al.[69] | https://github.com/almaan/stereoscope |

## RESOURCE AVAILABILITY

### Lead contact

Requests for further information and/or resources and reagents should be directed to and will be addressed by the lead contact: Dr. Stefania Giacomello (stefania.giacomello@scilifelab.se).

### Materials availability

This study did not generate new materials.

### Data and code availability

- scRNA seq and spatial transcriptomics data are available at Asp et al. (2019) and Mendeley Data: https://doi.org/10.17632/mbvhhf8m62.2. Background ST maps grobs data are available at Mendeley Data: https://doi.org/10.17632/xgs5yf9zch.1.
- Code is available at GitHub: https://github.com/giacomellolab/Human-Prenatal-Cardiomyocytes.
- Any additional information required to reanalyze the data reported in this paper is available from the lead contact upon request.

## EXPERIMENTAL MODEL AND SUBJECT DETAILS

This study used *in silico* methods and previously reported materials.

## METHOD DETAILS

### Data

The exploration of prenatal CM phenotypes was based on sc-RNAseq and ST data from the *HDCA*.[16] In summary, data obtained from analyses of two hearts were analyzed. Data relating to one (of 6.5–7.0 PCW) were used for single-cell transcriptomic (scRNA-seq) analysis and data relating to the other (of 6.5 PCW) for ST analysis. These two hearts were considered to be biological replicates.

Using a 10X Genomics Chromium workstation, 3717 single-cell transcriptional profiles, with on average transcripts of 2900 genes and 11,000 unique transcripts per cell, were generated after quality trimming and filtering. The ST dataset consisted of 1515 individual spots (i.e., data points equivalent to microdissections, each containing ≈30 cells, with on average transcripts of ≈2100 genes and ≈4800 transcripts per cell.

The heart was sectioned consecutively in the transversal plane and ST analysis was performed on nine tissue sections at levels 0, 1, 115, 200, 360, 361, 520, 521, and 675.

### scRNA-seq analysis

The scRNA-seq analysis was performed using the Seurat package, version 4.0.0[68]. The whole material was analyzed first, then the three cardiomyocyte clusters were subclustered under the same conditions. A subset of cells expressing between 200 and 6000 features, with <50,000 counts and <20% mitochondrial content, was produced. The SCTransform function was used to regress out the influence of percent.mt, S.Score, and G2M.Score. Thereafter, 3675 cells remained for further analysis. After PCA (pcs = 30), the FindNeighbours (dims = 1:30) and FindClusters (resolution = 0.38) routines were run. For cluster visualization, we used UMAP (dims = 1:30). The three muscle clusters were subset and the Seurat analysis was rerun as before. The FindClusters routine was run, with 0.7 resolution. To test the robustness of the muscle subset analysis, the analysis was also performed with different numbers of principal components (pcs = 25 and pcs = 35), resulting in the same cluster distribution (Figure S1B). SAN cells were identified in a supervised manner by the simultaneous expression of *SHOX2*, *TBX10*, and *HCN4*.[36–38] To identify differentially expressed genes, pairwise comparisons of individual clusters against all other clusters were performed using the FindAllMarkers routine (settings: min.pct = 0.25; logfc.threshold = 0.25) and the Wilcoxon rank-sum test with Bonferroni correction for multiple testing included in the Seurat package.

### GO characterization

GO characteristics of gene clusters were determined using the clusterProfiler package (version 3.14.3)[70] for all DE genes with an average value of log2FC above zero, and adjusted $p < 0.01$. The compareCluster function was used, with pvalueCutoff = 0.05.

### Cardiomyocyte cell type validation

The cardiomyocyte types characterized by GO and differential gene expression profiles were validated according to their spatial expression in spatial microdissected transcriptomic maps with barcoded regions of 100 μm in diameter that limited the resolution to ≈10–40 cells. The grid was projected on the tissue section image, enabling morphological localization of the cluster expressions.

To deconvolute spatial locations of the CM clusters, identified using scRNA-seq data, and the original non-CM single-cell clusters from the *HDCA* in the ST map, we used the AUCell algorithm, which identifies enriched gene sets in scRNA-seq data.[71] For each CM cluster identified using scRNA-seq data, we defined the active gene set as the top 12 differentially expressed genes or the marker genes for the SAN. The **AUCellbuildRankings** function was applied to the ST dataset, to build the "rankings" for each ST spot, i.e., expression-based ranking for all the expressed genes in each spot. Then the **AUCellcalc AUC** function was used to calculate whether a critical subset of the input gene set was enriched within the expressed genes for each ST spot. The AUC function thus represents proportions of expressed genes in the ST spot, and their expression relative to other genes in it. In this way, the population of cells present in the ST spot can be explored, according to the gene set's expression. To validate the method, cross-correlation was applied to the same scRNA-seq and ST data analyzed using the Stereoscope method (15 tsne-determined clusters with Seurat 2.3.4)[16,69]. Figure S6 shows correlations between Stereoscope and AUC (A), Stereoscope and Stereoscope (B) and AUC and AUC (C) data. Figure S6D shows AUC-AUC correlation for the 17 clusters identified with UMAP (Seurat 4.0.0) in this work. Figure S6E shows AUC-AUC correlation for the nine muscle clusters analyzed in this study. Crosses indicate correlations with $p \geq 0.01$. Figure S6 shows that deconvolution using the AUC method discriminates between cells in a manner similar to the Stereoscope method and that the different CM types can be deconvoluted.

As dynamics of ventricular and atrial CMs differ, results for the two types of CM are presented separately.

### L-R crosstalk

The L-R crosstalk between different cell types was analyzed using the cellphoneDB package.[44] The standard method was used involving 100 permutations for each interaction pair in all cells from which mean is calculated in cluster x (molecule 1) and mean in cluster 2 (molecule 2). Anticipating random clusters the resulting null-distribution is used to determine where the observed mean is located. Result precision was set to 2. After 100 iterations, L-R pairs between cell types were identified with significance set at $p < 0.01$.

## QUANTIFICATION AND STATISTICAL ANALYSIS

Analysis was done with the R Stats package. Continuous data were analyzed with Student's *t* test or ANOVA followed by pairwise.t test. Categorical data were analyzed with ChiSquare test or Kruskal Wallis test.